PHYSICAL REVIEW B **112**, 115411 (2025)

Coupling between ferroelectricity, Rashba splitting, and band topology enabled by quadruple-well ferroelectrics

Xin Jin,[1] Jinbo Pan,[1,2] Yu-Yang Zhang,[1,*] and Shixuan Du[1,2,†]

[1]University of Chinese Academy of Sciences and Institute of Physics, Chinese Academy of Sciences, Beijing 100049, China
[2]Songshan Lake Materials Laboratory, Dongguan, Guangdong 523808, China

(Received 18 April 2025; revised 29 July 2025; accepted 20 August 2025; published 8 September 2025)

The Rashba effect, characterized by spin splitting in band structures and helical spin textures, plays a pivotal role in various spintronics. However, the nonvolatile modulation of the Rashba splitting magnitude α_R in a single material, which potentially gives rise to novel spintronics, still remains unrealized. Here by using density-functional-theory calculations, we theoretically demonstrate the quadruple-well ferroelectrics (FEs) $(\mathrm{Pt,Pd})_2\mathrm{Sn}_2\mathrm{Te}_6$, featured by four stable FE states, ±high- and ±low-polarization states (±HP and ±LP states), and enable the nonvolatile interconversion between strong and weak Rashba splitting mediated by the HP-LP transformation. Given that the band anticrossing, the typical feature of topologically nontrivial band structures, is associated with the strong Rashba splitting, such HP-LP transformation also enables the topological phase transition between a topological insulator and a conventional semiconductor. The intercoupling between ferroelectricity, Rashba splitting, and band topology provides a unique mechanism for modulating the α_R and topological characteristics in a nonvolatile way, paving ways for various novel spintronics and topological electronics.

DOI: 10.1103/pp48-d63c

I. INTRODUCTION

The intercoupling of distinct properties in a same material unit is of great significance for both fundamental research and practical applications. Rashba ferroelectrics (FEs), exhibiting coupled FE orderings and Rashba effect, are such typical materials [1]. The Rashba effect is a unique form of spin-orbit coupling (SOC) interactions exhibited in materials where inversion symmetry is broken while specific symmetry (C_{3v}, C_{4v}, D_6, or C_{6v}) is maintained, characterized by the spin splitting in band structure and associated helical spin texture with spin-momentum locking [2–9]. The Rashba FEs enables the reversal of the spin texture by flipping the FE polarization, making such materials desired in various spintronics such as spin field-effect transistors (spin-FETs) [4,10], spin-charge converters [11–13], spin-orbit torques [6,14,15], etc. Bulk GeTe was the first Rashba FEs verified in experiment [11,12,16–18]; subsequently, several bulk and two-dimensional (2D) FE materials were also predicted to be Rashba FEs [10,19–21], providing ideal platforms for studying the couplings between FE orderings and Rashba splitting.

Despite that the reversal of spin textures is enabled by Rashba FEs, the nonvolatile manipulation of the Rashba splitting magnitude, characterized by the Rashba coefficient α_R, remains unrealized in Rashba FEs. Given that the key properties of some spintronics, such as spin-charge conversion efficiency, are proportional to α_R [3], the nonvolatile manipulation of α_R would enable the design of novel multifunctional spintronics. It should be noted that the nonvolatile modulation of α_R cannot be achieved in the conventional double-well FEs since the polarization-up/-down states exhibit the same band structures, i.e., the same Rashba splitting. To the best of our knowledge, the nonvolatile modulation of α_R was only predicted in LiAlTe_2, where the inequivalence between the two polarized states allows the polarization modulation of α_R, but also prohibits the reversal of spin texture [22]. While the recently predicted 2D quadruple-well FEs $(\mathrm{Pt,Pd})_2\mathrm{Sn}_2(\mathrm{Se,Te})_6$ [23] shed light on the nonvolatile modulation of both α_R and spin-texture direction. Such materials possess four distinct polarization states: ±low-/high-polarization (±LP/HP) states, where the LP and HP states show different magnitudes of polarizations and atomic configurations, indicating the α_R of their band structures could be different. The transformation between ±LP and ±HP states under electric field would further enable the nonvolatile modulation of α_R, as well as the spin-texture direction.

The potential nonvolatile modulation of α_R enabled by 2D quadruple-well FEs also opens up opportunities to tune their topological orders. As proposed by Acosta *et al.*, materials characterized by strong Rashba splitting ($\alpha_R >\sim 1.0$ eV Å) generally possess band anticrossing in their electronic structures, which is absent for weak Rashba splitting [24]. Given that the band anticrossing is the typical feature of nontrivial band topology, the nonvolatile modulation of α_R from strong to weak in 2D quadruple-well FEs, if realized, would simultaneously tune their band topologies from nontrivial to trivial characteristics. Previously the FE modulation of topological order was predicted in antiferroelectric alkali-MgBi [25] or 2D topological (or trivial) insulator/FE heterostructures [26–28], but was absent in pure FEs since the exact

---

[*] Contact author: zhangyuyang@ucas.ac.cn

[†] Contact author: sxdu@iphy.ac.cn

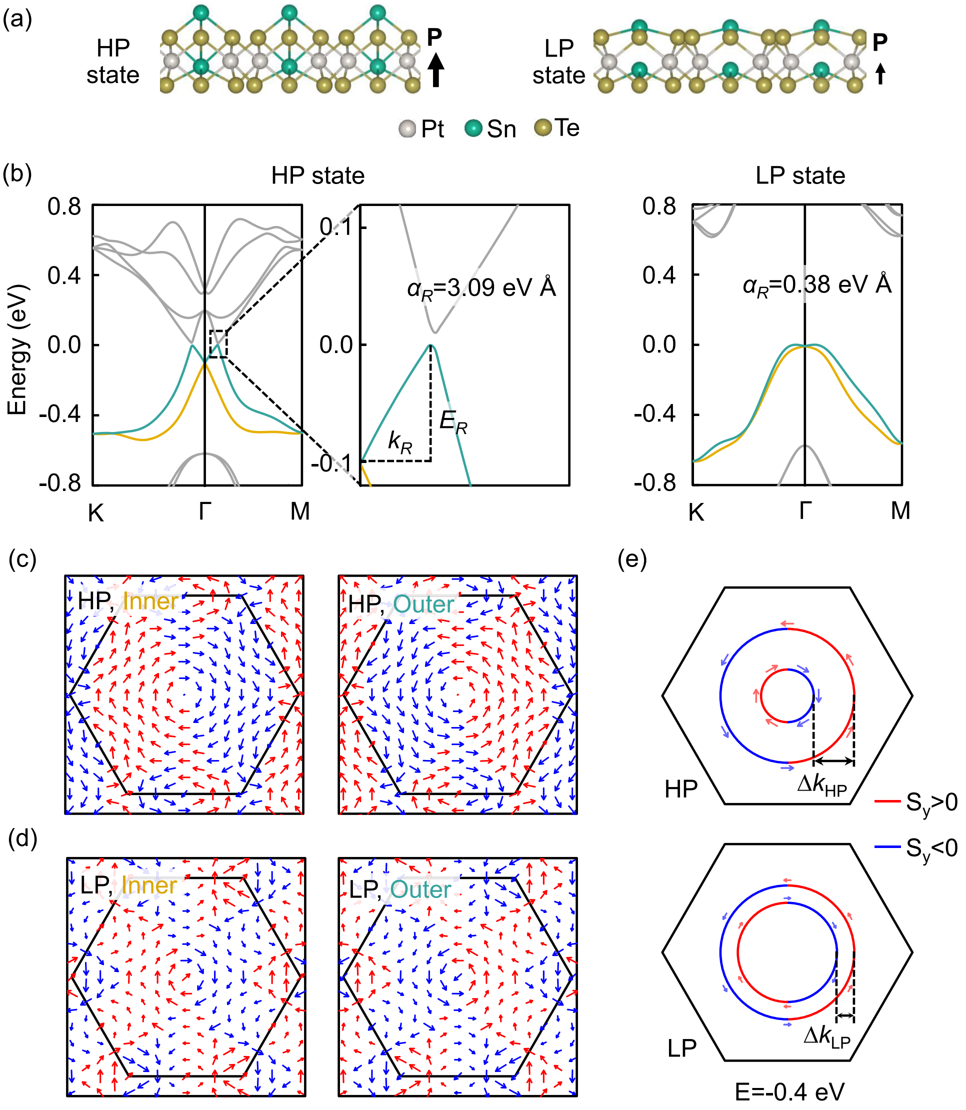

FIG. 1. Electronic properties of 2D quadruple-well ferroelectric $Pt_2Sn_2Te_6$. (a) Atomic structures of the +HP and +LP states of $Pt_2Sn_2Te_6$, respectively. (b) Band structures of HP- and LP-$Pt_2Sn_2Te_6$, respectively. The outer and inner bands of the splitVBM are marked in green and yellow, respectively. (c), (d) The spin textures of the inner and outer branches of the VBM of HP- and LP-$Pt_2Sn_2Te_6$, respectively (only in-plane components are shown). Blue and red represent S_y is negative and positive, respectively. (e) Fermi contour of $Pt_2Sn_2Te_6$ in HP and LP state, respectively. The energy of the fermi contour is 0.4 eV below the Fermi level. (Note: the Fermi level locates at the VBM.)

same electronic structures of the FE up/down states prohibit such possibilities. The 2D quadruple-well FEs provide opportunities to modulate the topological order through HP-LP transformation, which may lead to novel topological electronics.

In this paper, by using density-functional-theory calculations, we theoretically explore the possibilities of nonvolatile manipulation of the Rashba splitting magnitude, as well as band topology in the 2D quadruple-well FE $(Pt, Pd)_2Sn_2(Se, Te)_6$. We find that within the four 2D quadruple-well FEs, Pt_2 Sn_2Te_6 ($Pd_2Sn_2Te_6$) are Rashba FEs and exhibit distinct Rashba splitting magnitude in their HP and LP states: $\alpha_R = 3.09$ (1.28) and 0.38 (0.34) eV Å for HP and LP states, respectively, indicating the nonvolatile strong-weak Rashba splitting interconversion is enabled by the HP-LP transformation. Given the above framework, we further studied the band topology of $(Pt, Pd)_2Sn_2(Se, Te)_6$ and found the HP-LP transformation also leads to the interconversion between topological insulators and conventional semiconductors, i.e., topological phase transition, in $(Pt, Pd)_2Sn_2Te_6$ and $Pt_2Sn_2Se_6$. Such unique intercoupling between ferroelectricity, Rashba SOC, and band topology enables the design of various new multifunctional devices such as spin-FETs integrated with multistate memory, efficiency tunable spin-charge converters, topological field-effect transistors, etc., providing perspectives for the design of next-generation functional devices.

II. RESULTS AND DISCUSSION

A. Ferroelectricity-Rashba splitting coupling in 2D quadruple-well FEs

We first investigated the electronic properties of $(Pt, Pd)_2Sn_2(Se, Te)_6$ to verify whether they are quadruple-well Rashba FEs, that is, both LP and HP should be featured by energy bands with sizable Rashba splitting, as well as helical spin textures. Here we take $\mathrm{Pt_2Sn_2Te_6}$ as an example to demonstrate its properties, while the results of $\mathrm{Pd_2Sn_2Te_6}$ and $\mathrm{(Pt, Pd)_2Sn_2Se_6}$ are shown in the Supplemental Material [29]. Figure 1(a) shows the atomic structures of the +HP and +LP states of $\mathrm{Pt_2Sn_2Te_6}$. Previous literature have shown that both HP and LP states of $\mathrm{Pt_2Sn_2Te_6}$ [as well as $\mathrm{Pd_2Sn_2Te_6}$ and $\mathrm{(Pt, Pd)_2Sn_2Se_6}$] are dynamically, thermodynamically, and thermally stable [23]. Clearly, the major difference between the HP and LP states is the displacements of the Sn atoms relative to the Te plane, which results in polarizations of different magnitudes. The Sn displacements break the inversion symmetry of $\mathrm{Pt_2Sn_2Te_6}$, combined with the SOC contributed by the heavy elements, which will lead to the Rashba-splitted bands in principle. As shown in Fig. 1(b), the band structures of $\mathrm{Pt_2Sn_2Te_6}$ (SOC considered) show that the valence band maximum (VBM) of both HP and LP states are split into two subbands, as marked in green (outer band) and yellow (inner band), respectively. The corresponding spin textures are shown in Figs. 1(c) and 1(d), showing the characteristic chiral spin texture: The inner and outer bands exhibit clockwise and anticlockwise chirality near the Γ point, respectively, for both HP and LP states, demonstrating $\mathrm{Pt_2Sn_2Te_6}$ is indeed quadruple-well Rashba FEs. Among the other three quadruple-well FEs, $\mathrm{Pd_2Sn_2Te_6}$ is also verified to be quadruple-well Rashba FEs, as shown in Supplemental Material [29] Fig. S1. For $\mathrm{Pt_2Sn_2Se_6}$, the HP-$\mathrm{Pt_2Sn_2Se_6}$ exhibit sizable Rashba splitting, while its LP state shows nearly zero Rashba splitting [Figs. S2(a) and S2(b)] [29]; $\mathrm{Pd_2Sn_2Se_6}$ in both HP and LP states show no Rashba splitting, thus $\mathrm{(Pt, Pd)_2Sn_2Se_6}$ does not meet the criteria to be quadruple-well Rashba FEs [30–45].

Quantitatively, the magnitude of Rashba splitting is characterized by the Rashba coefficient α_R, calculated by $\alpha_R = 2E_R/k_R$, where E_R is spin splitting and k_R is momentum offset, as shown in Fig. 1(b). Here we adopt the isotropic Rashba splitting approximation; the contribution of the high-order Rashba term is also neglected. A Detailed discussion about the anisotropic Rashba splitting, as well as the contribution of the high-order Rashba term in HP-/LP-$\mathrm{(Pt, Pd)_2Sn_2Te_6}$, are shown in the Supplemental Material [29]. The as-calculated α_R of HP- and LP-$\mathrm{Pt_2\,Sn_2Te_6}$ ($\mathrm{Pd_2\,Sn_2\,Te_6}$) is 3.09 (1.28) and 0.38 (0.34) eV Å, belonging to the strong and weak Rashba splitting as classified in previous literature [24]. Furthermore, the transformation between the HP and LP states of $\mathrm{(Pt, Pd)_2Sn_2Te_6}$ can be achieved by applying an external electric field, where the transformation barrier is around 0.3 eV/f.u. [23]. Such results demonstrate that $\mathrm{Pt_2Sn_2Te_6}$ and $\mathrm{Pd_2Sn_2Te_6}$ enable the nonvolatile electrical conversion between strong and weak Rashba splitting, mediated by the transformation between their HP and LP states. We note such properties are unique behaviors of $\mathrm{Pt_2Sn_2Te_2}$ and $\mathrm{Pd_2Sn_2Te_6}$: another well-known quadruple-well FE $\mathrm{CuInP_2S_6}$ [46] lacks heavy elements, thus its SOC is relatively weak, i.e., the Rashba splitting is absent in $\mathrm{CuInP_2S_6}$; while for conventional double-well FEs, as we stated above, the electronic structures of their polarization-up and -down states are exactly the same, prohibiting the modulation of α_R through ferroelectric reversal.

The effect of the distinct Rashba splitting of HP- and LP-$\mathrm{Pt_2Sn_2Te_6}$ on their electronic properties can be characterized more intuitively by investigating their Fermi contour. Figure 1(e) shows the Fermi contour at 0.4 eV below the Fermi level of the HP and LP states of $\mathrm{Pt_2Sn_2Te_6}$. Clearly, the HP-$\mathrm{Pt_2Sn_2Te_6}$ exhibits more significant difference between the radius of the outer and inner Fermi contour, as marked by Δk_{HP} in Fig. 1(e), compared to that of LP-$\mathrm{Pt_2Sn_2Te_6}$ (i.e., Δk_{LP}). As a direct consequence of the different Δk_{HP} and Δk_{LP}, HP- and LP-$\mathrm{Pt_2Sn_2Te_6}$ will exhibit different efficiency in spin-charge conversion [10,47]. Additionally, in spin-FET, the spin precession angle θ of the channel electron is proportional to α_R of its host materials, while the channel current relies on θ, thus the nonvolatile modulation of the channel current is expected in $\mathrm{(Pt, Pd)_2Sn_2Te_6}$-based spin-FET mediated by the transformation between their HP and LP states. We will discuss these points in detail in the following sections.

B. Ferroelectricity-band topology coupling in 2D quadruple-well FEs

As we stated above, the strong-weak Rashba splitting interconversion enabled by HP-LP transformation also provides opportunities to tune the band topology of 2D quadruple-well Rashba FEs. As reported in ref. [24], the band anticrossing is a hallmark of strong Rashba splitting: the band with anticrossing is typically more dispersive, which generally leads to large spin splitting with small momentum offset, i.e., strong Rashba splitting, as shown schematically in Fig. 2(a), left panel, while a band lacking anticrossing is generally less dispersive and thus results in weak Rashba splitting. Inspired by the strong and weak Rashba splitting exhibited by HP- and LP-$\mathrm{Pt_2Sn_2Te_6}$, we further investigated its band anticrossing characteristic. As shown in Fig. 2(b), the band structure of HP-$\mathrm{Pt_2Sn_2Te_6}$ shows apparent band anticrossing: for $k < k_R$, the VBM [conduction band minimum (CBM)] is mainly contributed by the Sn p_{xy} (Sn sp_z) orbitals; while for $k > k_R$, the character of the orbital contributing to the VBM (CBM) turns into Sn sp_z (Sn p_{xy}), matching with the strong Rashba splitting exhibited in HP-$\mathrm{Pt_2Sn_2Te_6}$. Conversely, such a feature is absent in the LP-$\mathrm{Pt_2Sn_2Te_6}$ [Fig. 2(c)], consistent with its weak Rashba splitting.

Given that the band anticrossing is a typical feature of topological insulators, we further investigated the topological properties of HP- and LP-$\mathrm{Pt_2Sn_2Te_6}$. Theoretically, the topological properties of materials with time-reversal symmetry (i.e., nonmagnetic) are typically characterized by its $\mathbf{Z_2}$ invariant, which can be obtained by tracing the evolution of the Wannier charge center. When the evolution lines of the Wannier charge center, i.e., Wilson loop, are crossed by an arbitrary horizontal reference line an odd number of times, then $\mathbf{Z_2} = 1$, corresponding to the topologically nontrivial case, otherwise $\mathbf{Z_2} = 0$, i.e., topologically trivial [48]. The calculated Wilson loops of $\mathrm{Pt_2Sn_2Te_6}$ in HP and LP states are shown in Fig. S4(a) [29]; clearly for HP-$\mathrm{Pt_2Sn_2Te_6}$, the reference line crosses the Wilson loop a single time, as marked by the red dot, indicating HP-$\mathrm{Pt_2Sn_2Te_6}$ is topologically nontrivial, while LP-$\mathrm{Pt_2Sn_2Te_6}$ is topologically trivial. The topological order of the HP/LP states of $\mathrm{Pt_2Sn_2Te_6}$ can be further checked by calculating their edge states. As shown in Fig. 2(d), a pair of edge states around the Γ point emerge within the bulk gap of HP-$\mathrm{Pt_2Sn_2Te_6}$, while the edge states

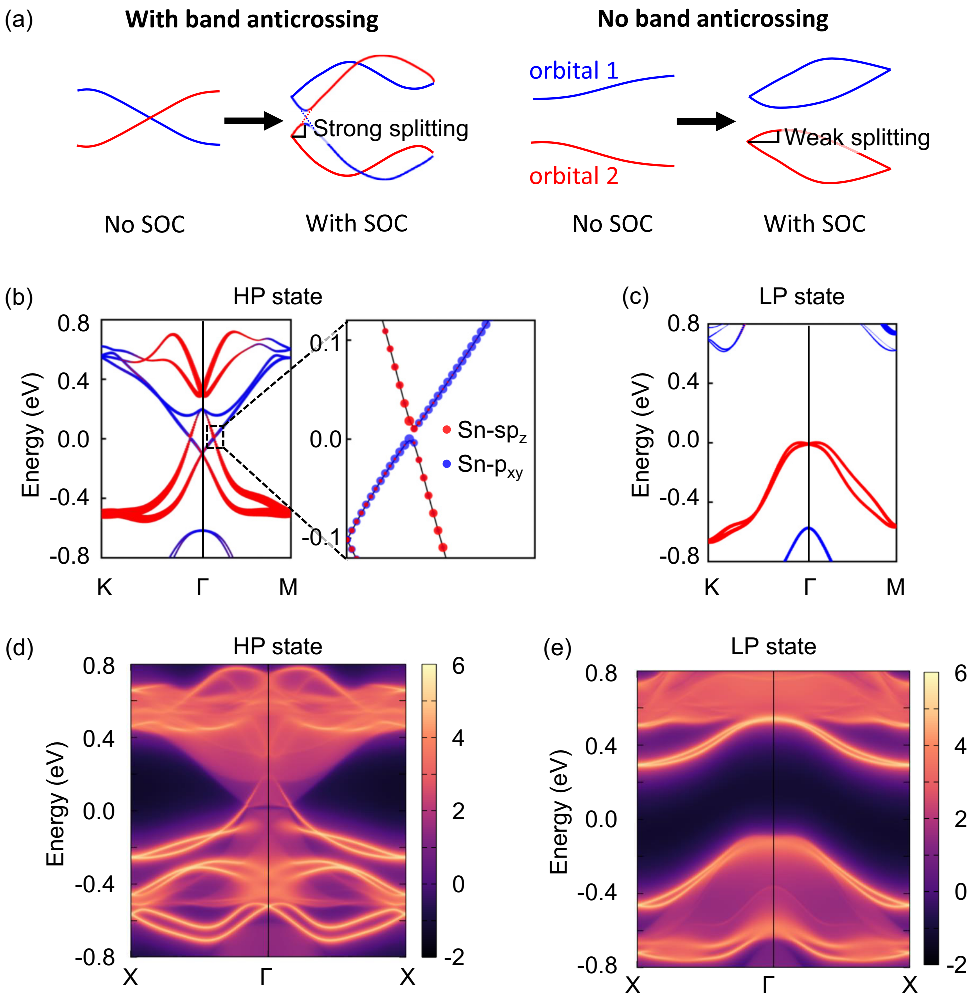

FIG. 2. Topological properties of 2D quadruple-well ferroelectric $Pt_2Sn_2Te_6$. (a) Schematic of the relations between Rashba splitting and band anticrossing, adapted from ref. [24]. (b), (c) Projected band structures of HP- and LP-$Pt_2Sn_2Te_6$, respectively, where the red and blue represent the sp_z and p_{xy} orbitals of Sn atoms. (d), (e) Edge states of HP- and LP-$Pt_2Sn_2Te_6$, respectively.

are absent in the gap of LP-$Pt_2Sn_2Te_6$ as shown in Fig. 2(e), indicating the HP-/LP-$Pt_2Sn_2Te_6$ are topologically nontrivial/trivial, respectively. The distinct band topology of HP- and LP-$Pt_2Sn_2Te_6$ originates from the variation of Sn coordination in their atomic configurations. As shown in Figs. S6(a) and S6(b) [29], the top and bottom Sn atoms in HP-$Pt_2Sn_2Te_6$ are three- and six-coordinated to the Te atoms, thus they contribute different Sn orbitals to the VBM/CBM of HP-$Pt_2Sn_2Te_6$ as shown in Fig. S6(c) [29], resulting in a band anticrossing characteristic; While in LP-$Pt_2Sn_2Te_6$, both the top and bottom Sn atoms show the $SnTe_3$ coordination [Figs. S6(d) and S6(e)] [29], causing the same Sn orbital contribution to the VBM of LP-$Pt_2Sn_2Te_6$ [Fig. S6(f)] [29], finally leading to trivial band structures.

The band topology of the other three quadruple-well FEs were also investigated. $Pd_2Sn_2Te_6$ and $Pt_2Sn_2Se_6$ exhibit electronic properties similar to $Pt_2Sn_2Te_6$: the band anticrossing characteristic of Sn sp_z and p_{xy} emerges in its HP state, but vanishes in the LP state [Figs. S3(a)–S3(d)] [29], leading to the topological nontrivial/trivial band in its HP/LP state, respectively, as verified by their Wilson loops [Figs. S4(b) and S4(c)] [29] and edge states [Figs. S5(a)–S5(d)] [29]. For $Pd_2Sn_2Se_6$, the band anticrossing characteristics do not appear for both the HP and the LP states [Figs. S3(e) and S3(f)] [29]. The corresponding Wilson loops [Fig. S4(d)] [29] and edge states [Figs. S5(e) and S5(f)] [29] further demonstrates that both HP- and LP-$Pd_2Sn_2Se_6$ are topological trivial. To summariz, in $(Pt, Pd)_2Sn_2Te_6$ and $Pt_2Sn_2Se_6$, the FE orderings are coupled to their band topology, enabling the nonvolatile interconversion between a topological insulator and a conventional semiconductor (i.e., topological phase transition) mediated by the HP-LP transformation. Such unique properties pave the way for novel topological electronics, such as topological field-effect transistors [49].

C. Design of novel spintronics based on 2D quadruple-well FEs

Beyond the topological electronics, the coupling between ferroelectricity and Rashba splitting also makes $(Pt, Pd)_2Sn_2Te_6$ promising materials for multifunctional spintronics. Here we take the $Pt_2Sn_2Te_6$ as an example for demonstration. The spin-FET proposed by Datta and Das is a typical spintronic exploited by the Rashba effects, where Rashba and ferromagnetic materials are used as channel materials and source/drain electrodes, respectively [50–52].

Obviously $Pt_2Sn_2Te_6$ can serve as a channel material on spin-FETs. Due to the spin-momentum locking, the spins of the electrons in the spin-FET channel will precess when the electron propagates, which further controls the channel current of the spin-FET. The spin precession angle is given by [50,53,54]

$$\theta = \frac{2\alpha_R m^* L}{\hbar^2},$$

where α_R is the Rashba coefficient, m^* is the carrier effective mass, which can be calculated by $m^* = \hbar^2 k_R^2/2E_R$, and L is the channel length. Such formulas are originally derived based on a 2D electron gas model, but are effective for various Rashba ferroelectrics [16,55,56]. The calculated carrier effective masses of the HP- and LP-$Pt_2Sn_2Te_6$ are $0.16m_e$ and $0.85m_e$, respectively. Here we set the angle θ of the +LP state as $\pi/2$, and the corresponding channel length is calculated to be 1.85 nm. Such a value is much smaller than the typical spin diffusion length (hundreds of nanometers to several micrometers) [51,57,58], thus the coherent spin transport is expected to be dominant. The calculated spin precession angle for the ±LP, ±HP states of $Pt_2Sn_2Te_6$ are

$$\theta(+\text{LP}) = 0.5\pi, \quad \theta(-\text{LP}) = -0.5\pi,$$
$$\theta(+\text{HP}) = 0.77\pi, \quad \theta(-\text{HP}) = -0.77\pi.$$

The spin-FET channel current relies on θ in a sinusoidal form as $J = J_0(1+\sin\theta)/2$ [10,54,59,60], thus the distinct channel current is expected for the ±LP and ±HP states, as shown by the top panel of Fig. 3(a). Furthermore, the interconversion among the ±HP and ±LP states of $Pt_2Sn_2Te_6$ can be achieved by applying a vertical electric field, i.e., gate voltage. Such characteristics bring out a new type of spin-FET, where nonvolatile mutistate memory is combined with the "computation" function in spin-FET, making it promising in fields such as in-memory computation, neuromorphic electronics, etc. [61–63]. It should be noted that in real scenarios, the α_R of the channel material will also be modulated by the gate voltage (Fig. S7) [29], which will lead to a longer spin-FET channel length [55]; however, the basic working mechanism would remain the same as we stated here.

The strong-weak Rashba splitting interconversion induced by HP-LP transformation in $Pt_2Sn_2Te_6$ also enables the modulation of the efficiency of spin-charge interconversion. In charge-to-spin conversion, known as direct Rashba-Edelstein effect (DREE), an injected charge current along the x direction leads to the shift of Fermi contour along k_x, thus inducing spin accumulation $\delta S\uparrow$ ($\delta S\downarrow$) along the y direction for the outer (inner) Fermi contour [3,6]. The induced net magnetization, $M_{\text{DREE}} = \delta S\uparrow - \delta S\downarrow$, can be detected by measuring the magnetoresistance [64,65]. For $Pt_2Sn_2Te_6$, its HP state shows a more significant Fermi contour radius difference compared to the LP state [Fig. 1(e)], thus the same injected charge current, i.e., the same Δk_x, will lead to larger M_{DREE} in the HP-$Pt_2Sn_2Te_6$ compared to the LP state, as shown schematically in Fig. 3(b). The charge-to-spin conversion efficiency can then be tuned through the application of gate voltage mediated by HP-LP transformation.

In the spin-to-charge conversion (inverse Rashba-Edelstein effect, short for IREE), by injecting spin density along the y direction, typically generated by spin-pumping ferromagnetic resonance [6], the inner and outer Fermi contours will shift in the reverse direction along k_x, as shown schematically in the top panel of Fig. 3(c). The charge current contributed by the outer and inner Fermi contours, represented by Δk_x and $\Delta k_x'$ in Fig. 3(c), is proportional to their Fermi contour radii [10,47,66]. The net induced charge current follows:

$$j_C = \frac{e\hbar\Delta k}{2m}\langle\delta s\rangle,$$

where Δk represents the Fermi contour radius difference [10,47,66]. With the same injected spin density $\langle\delta s\rangle$, the more significant Δk of the HP-$Pt_2Sn_2Te_6$ will generate a larger charge current, i.e., exhibit larger spin-to-charge conversion efficiency, compared to the LP-$Pt_2Sn_2Te_6$, as shown schematically by Fig. 3(c). Quantitatively, the spin-charge interconversion efficiency is defined as the ratio of the injected spin (charge) current to the generated charge (spin) current, which requires calculating spin relaxation time and is not so practical for the density-functional theory calculations. However, the microscopic mechanism of the different performance of HP-/LP-$Pt_2Sn_2Te_6$ on spin-charge interconversion as stated here would still remain valid.

III. CONCLUSION

In conclusion, by using density-functional-theory calculations, we theoretically revealed the intercoupling between ferroelectricity, Rashba splitting, and band topology in quadruple-well ferroelectrics $(Pt, Pd)_2Sn_2(Se, Te)_6$. Such materials enable the nonvolatile interconversion between the strong and weak Rashba splitting, namely, $\alpha_R = 3.09$ (1.28) and 0.38 (0.34) eV Å for $Pt_2\,Sn_2Te_6$ ($Pd_2\,Sn_2Te_6$), mediated by the transformation between their HP and LP states. Moreover, considering the band anticrossing, a characteristic of nontrivial band topology, is a typical hallmark of strong Rashba splitting, the HP-LP transformation further enables the nonvolatile topological phase transition between topological insulators and conventional semiconductors in $(Pt, Pd)_2Sn_2Te_6$ and $Pt_2Sn_2Se_6$. Such unique couplings provide a mechanism to achieve the nonvolatile modulation of the Rashba splitting magnitude and band topology, exhibiting potential applications in novel functional devices such as spin-FETs with nonvolatile multistate memory, efficiency tunable spin-charge converters, topological field-effect transistors, etc.

ACKNOWLEDGMENTS

This work was supported by the National Natural Science Foundation of China (Grants No. 52250402 and No. 92477205), the National Key R&D program of China (Grant No. 2024YFA1207800), CAS Project for Young Scientists in Basic Research (YSBR-003), and the Fundamental Research Funds for the Central Universities.

The authors declare no competing interests.

DATA AVAILABILITY

The data that support the findings of this article are not publicly available upon publication because it is not

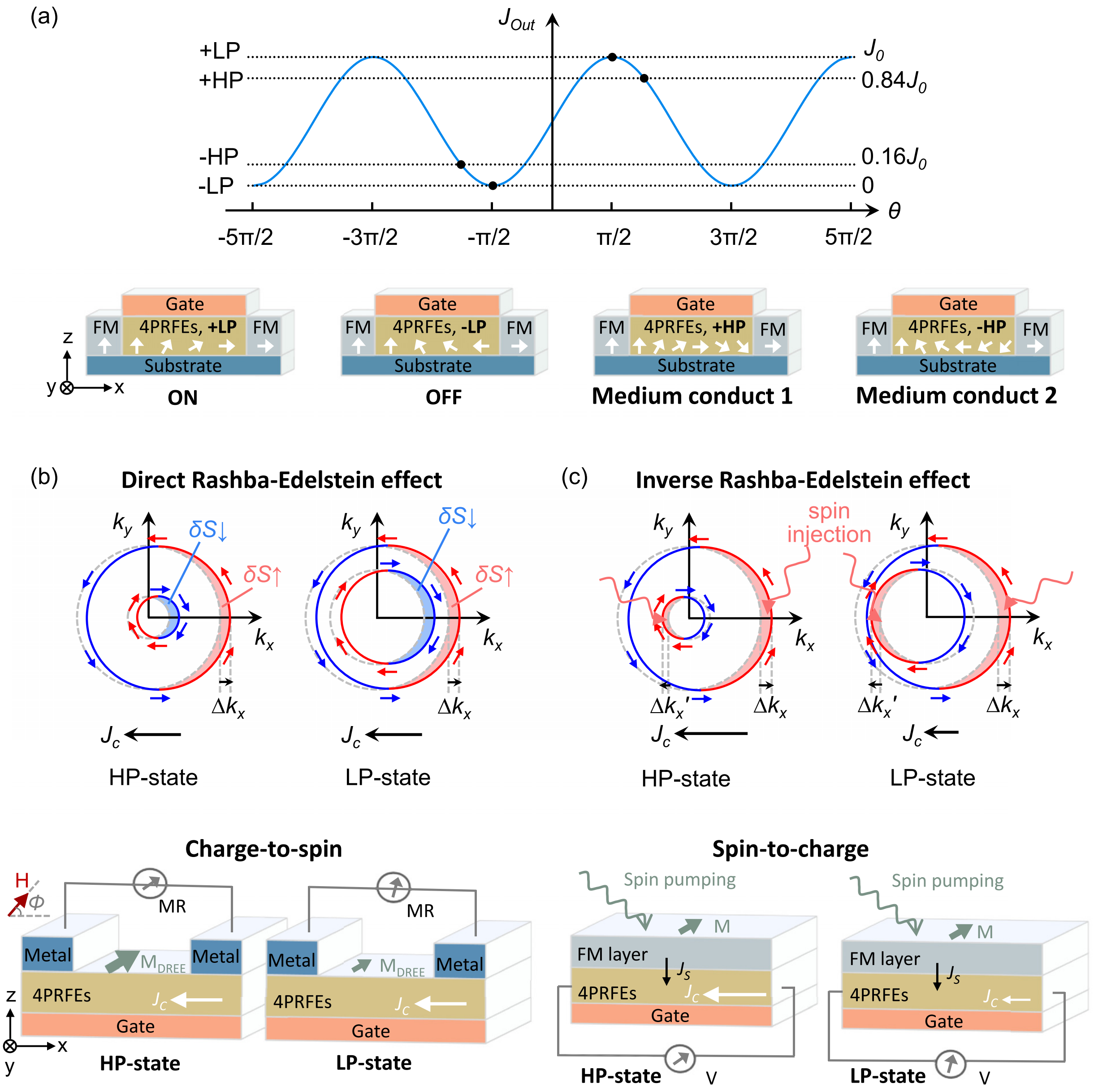

FIG. 3. Design of multifunctional spintronics based on 2D quadruple-well Rashba FEs (4PRFEs). (a) Schematic of the spin-FET integrated with nonvolatile multistate memory, where the 2D 4PRFEs are employed as channel materials. The top panel schematically shows the output channel current in such spin-FET where the 4PRFEs are in ±HP and ±LP states, respectively. The schematic of the device configuration is shown in the bottom panel. (b), (c) Schematic of the efficiency tunable spin-charge converter based on 2D 4PRFEs: (b) charge-to-spin conversion and (c) spin-to-charge conversion. The top panel shows the schematic of direct/inverse Rashba-Edelstein effect (DREE/IREE) in the HP and LP states, respectively, and the corresponding device configurations are shown in the bottom panel.

technically feasible and/or the cost of preparing, depositing, and hosting the data would be prohibitive within the terms of this research project. The data are available from the authors upon reasonable request.

---

[1] S. Picozzi, Ferroelectric Rashba semiconductors as a novel class of multifunctional materials, Front. Phys. **2**, 10 (2014).

[2] J. Chen, K. Wu, W. Hu, and J. Yang, Spin–orbit coupling in 2D semiconductors: A theoretical perspective, J. Phys. Chem. Lett. **12**, 12256 (2021).

[3] G. Bihlmayer, P. Noël, D. V. Vyalikh, E. V. Chulkov, and A. Manchon, Rashba-like physics in condensed matter, Nat. Rev. Phys. **4**, 642 (2022).

[4] H. C. Koo, S. B. Kim, H. Kim, T.-E. Park, J. W. Choi, K.-W. Kim, G. Go, J. H. Oh, D.-K. Lee, E.-S. Park, I.-S. Hong, and

K.-J. Lee, Rashba effect in functional spintronic devices, Adv. Mater. **32**, 2002117 (2020).

[5] A. Manchon, H. C. Koo, J. Nitta, S. M. Frolov, and R. A. Duine, New perspectives for Rashba spin–orbit coupling, Nat. Mater. **14**, 871 (2015).

[6] F. Trier, P. Noël, J.-V. Kim, J.-P. Attané, L. Vila, and M. Bibes, Oxide spin-orbitronics: Spin–charge interconversion and topological spin textures, Nat. Rev. Mater. **7**, 258 (2022).

[7] S. Vajna, E. Simon, A. Szilva, K. Palotas, B. Ujfalussy, and L. Szunyogh, Higher-order contributions to the Rashba-Bychkov effect with application to the Bi/Ag(111) surface alloy, Phys. Rev. B **85**, 075404 (2012).

[8] L. L. Tao and E. Y. Tsymbal, Perspectives of spin-textured ferroelectrics, J. Phys. D: Appl. Phys. **54**, 113001 (2021).

[9] C. Mera Acosta, L. Yuan, G. M. Dalpian, and A. Zunger, Different shapes of spin textures as a journey through the Brillouin zone, Phys. Rev. B **104**, 104408 (2021).

[10] J. Chen, K. Wu, W. Hu, and J. Yang, High-throughput inverse design for 2D ferroelectric Rashba semiconductors, J. Am. Chem. Soc. **144**, 20035 (2022).

[11] S. Varotto, L. Nessi, S. Cecchi, J. Sławińska, P. Noël, S. Petrò, F. Fagiani, A. Novati, M. Cantoni, D. Petti, E. Albisetti, M. Costa, R. Calarco, M. Buongiorno Nardelli, M. Bibes, S. Picozzi, J.-P. Attané, L. Vila, R. Bertacco, and C. Rinaldi, Room-temperature ferroelectric switching of spin-to-charge conversion in germanium telluride, Nat. Electron. **4**, 740 (2021).

[12] R. Fei and L. Yang, Room-temperature ferroelectric switching, Nat. Electron. **4**, 703 (2021).

[13] P. Noël, F. Trier, L. M. Vicente Arche, J. Bréhin, D. C. Vaz, V. Garcia, S. Fusil, A. Barthélémy, L. Vila, M. Bibes, and J.-P. Attané, Non-volatile electric control of spin–charge conversion in a $SrTiO_3$ Rashba system, Nature (London) **580**, 483 (2020).

[14] J. Jeon, S. W. Cho, O. Lee, J. Hong, J. Y. Kwak, S. Han, S. Jung, Y. Kim, H.-W. Ko, S. Lee, K.-J. Lee, and H. C. Koo, Field-like spin–orbit torque induced by bulk Rashba channels in GeTe/NiFe bilayers, NPG Asia Mater. **13**, 76 (2021).

[15] Y. Gu, Z. Zheng, L. Jia, S. Shi, T. Zhao, T. Zeng, Q. Zhang, Y. Zhu, H. Wang, and J. Chen, Ferroelectric control of spin-orbitronics, Adv. Funct. Mater. **34**, 2406444 (2024).

[16] D. Di Sante, P. Barone, R. Bertacco, and S. Picozzi, Electric control of the giant Rashba effect in bulk GeTe, Adv. Mater. **25**, 509 (2013).

[17] C. Rinaldi, S. Varotto, M. Asa, J. Sławińska, J. Fujii, G. Vinai, S. Cecchi, D. Di Sante, R. Calarco, I. Vobornik, G. Panaccione, S. Picozzi, and R. Bertacco, Ferroelectric control of the spin texture in GeTe, Nano Lett. **18**, 2751 (2018).

[18] J. Krempaský, S. Muff, J. Minár, N. Pilet, M. Fanciulli, A. P. Weber, E. B. Guedes, M. Caputo, E. Müller, V. V. Volobuev, M. Gmitra, C. A. F. Vaz, V. Scagnoli, G. Springholz, and J. H. Dil, *Operando* Imaging of all-electric spin texture manipulation in ferroelectric and multiferroic Rashba semiconductors, Phys. Rev. X **8**, 021067 (2018).

[19] A. Narayan, Class of Rashba ferroelectrics in hexagonal semiconductors, Phys. Rev. B **92**, 220101(R) (2015).

[20] R. Arras, J. Gosteau, H. J. Zhao, C. Paillard, Y. Yang, and L. Bellaiche, Rashba-like spin-orbit and strain effects in tetragonal $PbTiO_3$, Phys. Rev. B **100**, 174415 (2019).

[21] C. M. Acosta, A. Fazzio, G. M. Dalpian, and A. Zunger, Inverse design of compounds that have simultaneously ferroelectric and Rashba cofunctionality, Phys. Rev. B **102**, 144106 (2020).

[22] K. Y. Mak, L. L. Tao, and Y. Zhou, Polarization tunable Rashba effect in 2D $LiAlTe_2$, Appl. Phys. Lett. **118**, 062404 (2021).

[23] P. Li, L. Tao, X. Jin, G. Wan, J. Zhang, Y.-F. Zhang, J.-T. Sun, J. Pan, and S. Du, Nonvolatile multistate manipulation of topological magnetism in monolayer CrI_3 through quadruple-well ferroelectric materials, Nano Lett. **24**, 2345 (2024).

[24] C. Mera Acosta, E. Ogoshi, A. Fazzio, G. M. Dalpian, and A. Zunger, The Rashba scale: Emergence of band anti-crossing as a design principle for materials with large Rashba coefficient, Matter **3**, 145 (2020).

[25] B. Monserrat, J. W. Bennett, K. M. Rabe, and D. Vanderbilt, Antiferroelectric topological insulators in orthorhombic *A*MgBi compounds (*A*=Li, Na, K), Phys. Rev. Lett. **119**, 036802 (2017).

[26] J.-J. Zhang, D. Zhu, and B. I. Yakobson, Heterobilayer with ferroelectric switching of topological state, Nano Lett. **21**, 785 (2021).

[27] H. Bai, X. Wang, W. Wu, P. He, Z. Xu, S. A. Yang, and Y. Lu, Nonvolatile ferroelectric control of topological states in two-dimensional heterostructures, Phys. Rev. B **102**, 235403 (2020).

[28] A. Marrazzo and M. Gibertini, Twist-resilient and robust ferroelectric quantum spin Hall insulators driven by van der Waals interactions, npj 2D Mater. Appl. **6**, 30 (2022).

[29] See Supplemental Mateial at http://link.aps.org/supplemental/10.1103/pp48-d63c for calculation methods, Electronic properties of $Pd_2Sn_2Te_6$, and $(Pt, Pd)_2Sn_2Se_6$ Contributions of *s* and *p*orbitals of the Sn atoms to the band structures of $Pd_2Sn_2Te_6$ and, $(Pt, Pd)_2Sn_2Se_6$ Wannier charge center evolution and edge states of $Pd_2Sn_2Te_6$ and, $(Pt, Pd)_2Sn_2Se_6$, Local configurations of Sn atoms and atomically resolved projected band structures of HP- and LP-$Pt_2Sn_2Te_6$, Electric field modulation of the Rashba coefficient α_R of HP- and LP-$Pt_2Sn_2Te_6$, and Discussion on the anisotropy and high-order contribution of Rashba splitting. The Supplememtal Material also contains Refs. [30–45].

[30] G. Kresse, and J. Furthmüller, Efficiency of ab-initio total energy calculations for metals and semiconductors using a plane-wave basis set, Comput. Mater. Sci. **6**, 15 (1996).

[31] G. Kresse and J. Hafner, *Ab initio* molecular dynamics for liquid metals, Phys. Rev. B **47**, 558 (1993).

[32] G. Kresse and J. Hafner, *Ab initio* molecular dynamics for open-shell transition metals, Phys. Rev. B **48**, 13115 (1993).

[33] P. E. Blöchl, Projector augmented-wave method, Phys. Rev. B **50**, 17953 (1994).

[34] G. Kresse and D. Joubert, From ultrasoft pseudopotentials to the projector augmented-wave method, Phys. Rev. B **59**, 1758 (1999).

[35] J. P. Perdew, K. Burke, and M. Ernzerhof, Generalized gradient approximation made simple, Phys. Rev. Lett. **77**, 3865 (1996).

[36] J. Heyd, G. E. Scuseria, and M. Ernzerhof, Hybrid functionals based on a screened Coulomb potential, J. Chem. Phys. **118**, 8207 (2003).

[37] J. Heyd and G. E. Scuseria, Efficient hybrid density functional calculations in solids: Assessment of the Heyd–Scuseria–Ernzerhof screened Coulomb hybrid functional, J. Chem. Phys. **121**, 1187 (2004).

[38] A. V. Krukau, O. A. Vydrov, A. F. Izmaylov, and G. E. Scuseria, Influence of the exchange screening parameter on the performance of screened hybrid functionals, J. Chem. Phys. **125**, 224106 (2006).

[39] N. Marzari and D. Vanderbilt, Maximally localized generalized Wannier functions for composite energy bands, Phys. Rev. B **56**, 12847 (1997).

[40] I. Souza, N. Marzari, and D. Vanderbilt, Maximally localized Wannier functions for entangled energy bands, Phys. Rev. B **65**, 035109 (2001).

[41] A. A. Mostofi, J. R. Yates, Y.-S. Lee, I. Souza, D. Vanderbilt, and N. Marzari, WANNIER90: 685 A tool for obtaining maximally-localised Wannier functions, Comput. Phys. Commun. **178**, 685 (2008).

[42] A. A. Mostofi, J. R. Yates, G. Pizzi, Y.-S. Lee, I. Souza, D. Vanderbilt, and N. Marzari, An updated version of WANNIER90: A tool for obtaining maximally-localised Wannier functions, Comput. Phys. Commun. **185**, 2309 (2014).

[43] Q. Wu, S. Zhang, H.-F. Song, M. Troyer, and A. A. Soluyanov, WannierTools: An open-source software package for novel topological materials, Comput. Phys. Commun. **224**, 405 (2018).

[44] L. Fu, Hexagonal warping effects in the surface states of the topological insulator Bi_2Se_3, Phys. Rev. Lett. **103**, 266801 (2009).

[45] X. Yang, L. Qiu, Y. Li, H.-P. Xue, J.-N. Liu, R. Sun, Q.-L. Yang, X.-S. Gai, Y.-S. Wei, A. H. Comstock, D. Sun, X.-Q. Zhang, W. He, Y. Hou, and Z.-H. Cheng, Anisotropic nonlocal damping in ferromagnet/α-GeTe bilayers enabled by splitting energy bands, Phys. Rev. Lett. **131**, 186703 (2023).

[46] J. A. Brehm, S. M. Neumayer, L. Tao, A. O'Hara, M. Chyasnavichus, M. A. Susner, M. A. McGuire, S. V. Kalinin, S. Jesse, P. Ganesh, S. T. Pantelides, P. Maksymovych, and N. Balke, Tunable quadruple-well ferroelectric van der Waals crystals, Nat. Mater. **19**, 43 (2020).

[47] J. C. R. Sánchez, L. Vila, G. Desfonds, S. Gambarelli, J. P. Attané, J. M. De Teresa, C. Magén, and A. Fert, Spin-to-charge conversion using Rashba coupling at the interface between nonmagnetic materials, Nat. Commun. **4**, 2944 (2013).

[48] R. Yu, X. L. Qi, A. Bernevig, Z. Fang, and X. Dai, Equivalent expression of $\mathbb{Z}_2$ topological invariant for band insulators using the non-Abelian Berry connection, Phys. Rev. B **84**, 075119 (2011).

[49] X. Qian, J. Liu, L. Fu, and J. Li, Quantum spin Hall effect in two-dimensional transition metal dichalcogenides, Science **346**, 1344 (2014).

[50] S. Datta and B. Das, Electronic analog of the electro-optic modulator, Appl. Phys. Lett. **56**, 665 (1990).

[51] H. C. Koo, J. H. Kwon, J. Eom, J. Chang, S. H. Han, and M. Johnson, Control of spin precession in a spin-injected field effect transistor, Science **325**, 1515 (2009).

[52] D. Liang and X. P. A. Gao, Strong tuning of Rashba spin–orbit interaction in single InAs nanowires, Nano Lett. **12**, 3263 (2012).

[53] T. Koga, Y. Sekine, and J. Nitta, Experimental realization of a ballistic spin interferometer based on the Rashba effect using a nanolithographically defined square loop array, Phys. Rev. B **74**, 041302(R) (2006).

[54] S. Sugahara and J. Nitta, Spin-transistor electronics: An overview and outlook, Proc. IEEE **98**, 2124 (2010).

[55] J. Chen, K. Wu, W. Hu, and J. Yang, Tunable Rashba spin splitting in two-dimensional polar perovskites, J. Phys. Chem. Lett. **12**, 1932 (2021).

[56] B. Croes, A. Llopez, C. Tagne-Kaegom, B. Tegomo-Chiogo, B. Kierren, P. Müller, S. Curiotto, P. Le Fèvre, F. Bertran, A. Saúl, Y. Fagot-Revurat, F. Leroy, and F. Cheynis, Pushing the thickness limit of the giant Rashba effect in ferroelectric semiconductor GeTe, Nano Lett. **24**, 13224 (2024).

[57] S. Liang, H. Yang, P. Renucci, B. Tao, P. Laczkowski, S. McMurtry, G. Wang, X. Marie, J.-M. George, S. Petit-Watelot, A. Djeffal, S. Mangin, H. Jaffrès, and Y. Lu, Electrical spin injection and detection in molybdenum disulfide multilayer channel, Nat. Commun. **8**, 14947 (2017).

[58] J. Panda, M. Ramu, O. Karis, T. Sarkar, and M. V. Kamalakar, Ultimate spin currents in commercial chemical vapor deposited graphene, ACS Nano **14**, 12771 (2020).

[59] Y. H. Park, J. W. Choi, H.-j. Kim, J. Chang, S. H. Han, H.-J. Choi, and H. C. Koo, Complementary spin transistor using a quantum well channel, Sci. Rep. **7**, 46671 (2017).

[60] H. C. Koo, I. Jung, and C. Kim, Spin-based complementary logic device using Datta–Das transistors, IEEE Trans. Electron Devices **62**, 3056 (2015).

[61] C. Wang, Z. Si, X. Jiang, A. Malik, Y. Pan, S. Stathopoulos, A. Serb, S. Wang, T. Prodromakis, and C. Papavassiliou, Multi-state memristors and their applications: An overview, IEEE J. Emerging Sel. Top. Circuits Syst. **12**, 723 (2022).

[62] V. K. Sangwan and M. C. Hersam, Neuromorphic nanoelectronic materials, Nat. Nanotechnol. **15**, 517 (2020).

[63] B. Sun, S. Ranjan, G. Zhou, T. Guo, Y. Xia, L. Wei, Y. N. Zhou, and Y. A. Wu, Multistate resistive switching behaviors for neuromorphic computing in memristor, Mater. Today Adv. **9**, 100125 (2021).

[64] H. Nakayama, T. Yamamoto, H. An, K. Tsuda, Y. Einaga, and K. Ando, Molecular engineering of Rashba spin-charge converter, Sci. Adv. **4**, eaar3899 (2018).

[65] L. M. Vicente-Arche *et al.*, Spin–charge interconversion in $KTaO_3$ 2D electron gases, Adv. Mater. **33**, 2102102 (2021).

[66] S. Manipatruni, D. E. Nikonov, C.-C. Lin, T. A. Gosavi, H. Liu, B. Prasad, Y.-L. Huang, E. Bonturim, R. Ramesh, and I. A. Young, Scalable energy-efficient magnetoelectric spin–orbit logic, Nature (London) **565**, 35 (2019).